CrystEngComm

Themed issue: Crystal growth of nanomaterials

ROYAL SOCIETY
OF CHEMISTRY

PAPER
Maxim Gindele *et al.*
Generality of liquid precursor phases in gas diffusion-based
calcium carbonate synthesis

Generality of liquid precursor phases in gas diffusion-based calcium carbonate synthesis†

Maxim B. Gindele, Luisa Vanessa Steingrube and Denis Gebauer [iD] *

The ammonia diffusion method (ADM) is one of the most widely used strategies for the bioinspired synthesis of minerals. Herein, we present investigations of the mineralization mechanism using an advanced ADM to solve the limitations of the conventional ADM. This allows us to confirm the presence of liquid calcium carbonate precursor species in additive-free and polymer-stabilized gas diffusion systems, indicating that liquid–liquid phase separated species exhibit sufficient kinetic stability to be detected. Time-dependent experiments reveal the role of these precursor phases during the early stages of the crystallization process, demonstrating that liquid calcium carbonate mineral precursors play an important role in the precipitation pathway and must be generally considered for the interpretation of gas diffusion experiments, with and without additives. This discovery poses an important step in the understanding of how minerals are formed, highlighting that nonclassical mineralization processes must be considered for material synthesis. Last but not least, the advanced ADM may be useful for the exploration of the formation mechanism of other minerals than calcium carbonate, which are also of broad interest in the materials chemistry community.

Introduction

Gas diffusion-based synthesis methods are a useful tool to synthesize calcium carbonate and to investigate the effect of additives on the precipitation process, thereby providing new insights into biomineralization and biomimetic synthesis strategies.[1] In recent years, the most widely used diffusion-based method, the ammonia diffusion method (ADM),[2,3] has been utilized to synthesize calcium carbonate minerals for addressing questions in various research fields. The investigations of nucleation and crystal growth processes,[4,5] additive effects on the formation of calcium carbonate,[6–9] the synthesis and characterization of nanocomposites,[10–16] investigations regarding changes in material properties of crystals,[17] as well as syntheses of composite particles for potential use in cancer therapy,[18] have been carried out using the ADM. In addition, ADM has been used to investigate and characterize polymer-induced liquid precursor (PILP) phases.[19,20] Liquid precursor phases are essentially amorphous minerals with such a high degree of hydration that they appear and behave as a liquid and feature a liquid–liquid phase boundary to the mother solution. The liquid precursor species can densify to gel-like or solid amorphous calcium carbonates upon the loss of water. PILP phases are useful for explaining the complex "molded" non-equilibrium mineral morphologies found in organisms such as sea-urchins and present a promising way to new materials, for example for potential uses in biomedical applications[21,22] or as construction materials.[23] Recent results indicate that PILP phases are polymer-stabilized phases rather than polymer-induced phases, as liquid–liquid binodal demixing and the formation of dense liquid phases have been detected in additive-free aqueous calcium carbonate systems.[24,25] This can be explained by nonclassical nucleation models. It was shown that the formation of liquid intermediates in the absence of additives is defined by soluble, thermodynamically stable prenucleation clusters (PNCs),[26] where ion association is driven by the entropy gain of releasing hydration water molecules.[25] If supersaturation is increased and the corresponding liquid–liquid binodal limit is exceeded, PNCs can become phase-separated nanodroplets due to decreased cluster-dynamics upon increased calcium carbonate coordination numbers within the clusters. The formed nanodroplets can further aggregate to form larger, dense liquid precursor phases. It is still debated why certain additives can stabilize the liquid precursors. Current results indicate that additives, such as poly(carboxylates) or Mg^{2+} ions, favor the incorporation of water into the liquid and amorphous structures, preventing their dehydration toward the formation of solid amorphous calcium carbonate

Institute of Inorganic Chemistry, Leibniz University Hannover, Callinstraße 9, D 30167 Hannover, Germany. E-mail: gebauer@acc.uni-hannover.de

† Electronic supplementary information (ESI) available: Details of experimental procedure and characterization methods. See DOI: 10.1039/d1ce00225b

(ACC).[24,27] An alternative explanation could be the favorable incorporation of bicarbonate into the liquid phase.[28,29]

As mentioned above, liquid–liquid phase separation (LLPS) was proven numerous times in the case of calcium carbonate, with but also without additives.[24,29–31] However, liquid precursor phases received minor attention in the discussion of diffusion-based mineralization experiments so far, even if their liquid-like character is often useful for rationalizing results that are difficult to explain based on classical nucleation mechanisms.[32] Due to their fast transformation into more stable phases, such as solid ACCs or (metastable) crystals, liquid precursors are difficult to detect. Experimental strategies for the investigation of liquid mineral phases include cryogenic TEM studies,[30,33,34] NMR[29] and THz spectroscopy.[24] Another strategy is the investigation of the characteristics of solid amorphous phases that emerge from the dehydration of the initial liquid phases.[35] This strategy is also employed in this work using ADM as the method to synthesize calcium carbonate. Although ADM is not a new method and has been used for decades,[36] it was previously not employed for investigating transient precursor phases without additives, as usually volumes of several mL are used, resulting in low concentrations of the transient species which complicates their isolation and investigation. In addition, the transient species rapidly transform before it is possible to isolate them in the conventional ADM. Due to these limitations, so far, ADM has been mainly used to investigate more stable amorphous and crystalline minerals. In this work, we present several key advancements to solve these limitations of the ADM. The experiments are performed in droplets, thereby reducing the time necessary to remove the liquid and dry the transient species and thereby reducing the likelihood of their transformation before they can be investigated. In addition, performing experiments on wafers allows the transfer and investigation of all species present in the reaction solution at a certain time in the experiment. Another advantage of the mineralization in droplets is their beneficial economy: only small amounts of, potentially expensive, additives are necessary.

Our results confirm and visualize the occurrence, properties and kinetic stability of liquid calcium carbonate precursor species by employing the ADM, in the presence and absence of additives, underlining their general importance for the interpretation of ADM-based experiments. Furthermore, other carbonate minerals can be synthesized using the ADM,[37,38] where the mineralization mechanism and the potential occurrence of liquid intermediates can be studied using the experimental strategy presented herein in future.

Results and discussion

Characterization of polymer-stabilized precursor phases

ADM makes use of CO_2 diffusion into droplets of calcium chloride solution (Fig. 1).[9] After the desired reaction time, the solvent is removed, thereby transferring all species

Fig. 1 Schematic view of the droplet-based ammonia diffusion method. Experiments are performed in 20 μL $CaCl_2$ droplets on silica wafers. After the reaction is finished, the solvent is quickly removed using a filter paper. The precipitates on the wafer are then dried and investigated.

formed near or on the inner surface of the droplet, where calcium carbonate supersaturation is the highest, but also any species from the bulk of the droplet onto the wafer. As no further washing is performed, characterization of the dried wafers by SEM allows the investigation of all species present at this moment in the experiment. First, the effect of the polycarboxylate poly(acrylic acid) (PAA) on the precipitation of calcium carbonate was investigated. The influence of key parameters such as reaction time (1 h to 24 h), starting calcium chloride concentration (10 mM to 40 mM) and PAA concentration (0.01 to 1 g L^{-1}) was examined. Note that the formation of Ca–PAA coacervates and hydrogels is not

Fig. 2 Characterization of wafers after 1 h gas diffusion experiments with PAA additive. A) The film is visible to the naked eye, here shown for a PAA concentration of 0.5 g L^{-1}. B) ATR-FTIR spectra show that the precipitates on the wafer are ACC, confirmed by the band at 861 cm^{-1}, even for the highest additive concentration of 1 g L^{-1}. For comparison, spectra of pure ACC, pure PAA and the wafer are shown as well. Experimental conditions: 2 h gas diffusion experiment using 20 mM $CaCl_2$ solution with 1 g L^{-1} PAA. C) SEM image of the dried film on the wafer using 10 mM $CaCl_2$ and 0.01 g L^{-1} PAA and D) using 40 mM $CaCl_2$ and 0.01 mg L^{-1} PAA.

relevant in the systems of this work (Fig. S1†). For all investigated PAA concentrations, one hour experiments showed the formation of a macroscopic film on the surface of the droplet which was visible to the naked eye (Fig. 2A). ATR-FTIR characterization (Fig. 2B) of the dried film on the wafer shows that the precipitates are predominately ACC, confirmed by the band at 861 cm^{-1}. The dried film was further investigated using SEM (Fig. 2C and D), showing thin films of several 100 μm in their lateral dimension.

For high calcium and low PAA concentrations, particles were visible in addition to the film (Fig. 2D), showing the limited stability of the films for lower additive/calcium ratios. The morphology of the dried film showed differences in the top surface and the bottom surface of the film (Fig. S3†). The formation of liquid mineral phases on the surface of the droplet was expected, as PAA is known to stabilize PILPs;[23,39] however, the extent and macroscopic visibility of the liquid phase was not anticipated. The PILP films broke apart or dissolved when they were manipulated (Fig. S3 and Movie S1†) or upon attempts to isolate the films in their liquid state (Movie S2†). This is due to the liquid phase being only stable when in equilibrium with the mother phase. Liquid–liquid coexistence relies on the presence of two phases, so if the dense liquid is attempted to be isolated, it will fall apart.[9] The film can only be isolated when quickly dried and transferred into the solid state. Nevertheless, the liquid properties are evident if the structures of the dried liquid phases are closely examined (Fig. S4†).

Concentration-dependent experiments confirmed the stabilizing effect of PAA on the amorphous structures,[27,40] as for polymer contents higher than 0.5 g L^{-1}, no crystalline particles were visible in the 1 h experiments (Fig. S5†). Time-dependent experiments were used to resolve the evolution of the PILP film (Fig. S6†), showing that with increasing PAA concentration, films were detectable for several hours. If reaction times were long enough, however, the structures eventually crystallized and formed calcite particles with different morphologies and superstructures (Fig. S6†). In several experiments, semi-spherical calcite particles were detected (Fig. S7†), indicating that growth of the particles occurred from the precursor film, which can act as a substrate for particle growth, into the solution, accompanied by the densification of the precursor toward the crystalline phase. When the experiments were stopped before the growth into spherical particles was completed, semi-spherical structures were visible. Also, ACC particles already precipitated on the wafer when the film was still present on the surface of the solution (Movie S3†). This could be due to the simultaneous formation of ACC in the volume of the droplet, which then precipitates, or due to the release of ACC particles from the film into the solution.

### Liquid precursor phases in the absence of additives

The previously described conditions of gas diffusion-based CaCO$_3$ synthesis in droplets apparently favor the formation of continuous liquid precursor films. As liquid phases are also expected to exist in the additive-free calcium carbonate systems,[24,25] we investigated the crystallization without PAA using the same conditions. The PNC pathway allows the quantitative description of liquid–liquid phase separation (LLPS) in the aqueous calcium carbonate system.[25] We applied this quantitative model to estimate the time required for LLPS in the gas diffusion systems described here (ESI† discussion). Recent studies showed that the liquid–liquid binodal limit is defined by the solubility threshold of proto-structured ACCs.[24] Therefore, in general, from the solubility product of this ACC[26] and the known starting concentration of CaCl$_2$, the amount of carbonate necessary to exceed the binodal limit was calculated. Then, from previously established effects of different parameters in gas diffusion experiments,[3] the carbonate addition rate due to CO$_2$ in-diffusion was calculated. For the given experiments, the PNC model predicted that liquid–liquid phase-separation takes place on the timescale of 30 minutes, which was experimentally investigated.

The 1 h additive-free experiments yielded many different structures and particles (Fig. 3A and S8†). Most importantly and as predicted by the PNC model (ESI† discussion), also without polymeric additives, films of several 100 μm in diameter with smooth surfaces at the edges were visible (Fig. 3B).

These films were not observed close to amorphous and crystalline particles (Fig. 3A), which indicates that they served as the precursor phase to the denser amorphous and crystalline structures, and that the transformation took place by a dissolution–reprecipitation mechanism.[41] The presence of calcium carbonate in the films was supported by EDX (Fig. S10†). The large size of these films implies that a considerable amount of the calcium carbonate in the system was present in the form of these liquid precursors. It must be emphasized that the structures visible in the SEM are dried, solid residues of the once heavily hydrated species[42] formed on the surface of the droplet upon blotting and quick drying of the mother solution. The native state and the dynamics of these species could not be assessed due to their rapid transformation into more stable phases. However, the dried films allowed insights into the characteristics and transformation mechanisms of the precursor species. It was observed that the film covered the crystalline particles like a cloth (Fig. 3C), again visualizing the initial liquid- or gel-like properties of the detected phase. Time-dependent experiments showed the formation and evolution of the film (Fig. 3D–F). After 30 minutes, films of several hundred μm in their lateral dimension were visible (Fig. 3D). In some spots, the precursor phase already formed denser structures, resulting in holes in the film (Fig. S9†). In the 1 h experiments, additional amorphous and crystalline structures were present (Fig. 3E and S8†) whilst after two hours, only calcite particles were visible (Fig. 3F). The transformation of the film into particles was recorded (Fig. S11†), indicating a densification of the film toward the formation of 50 to
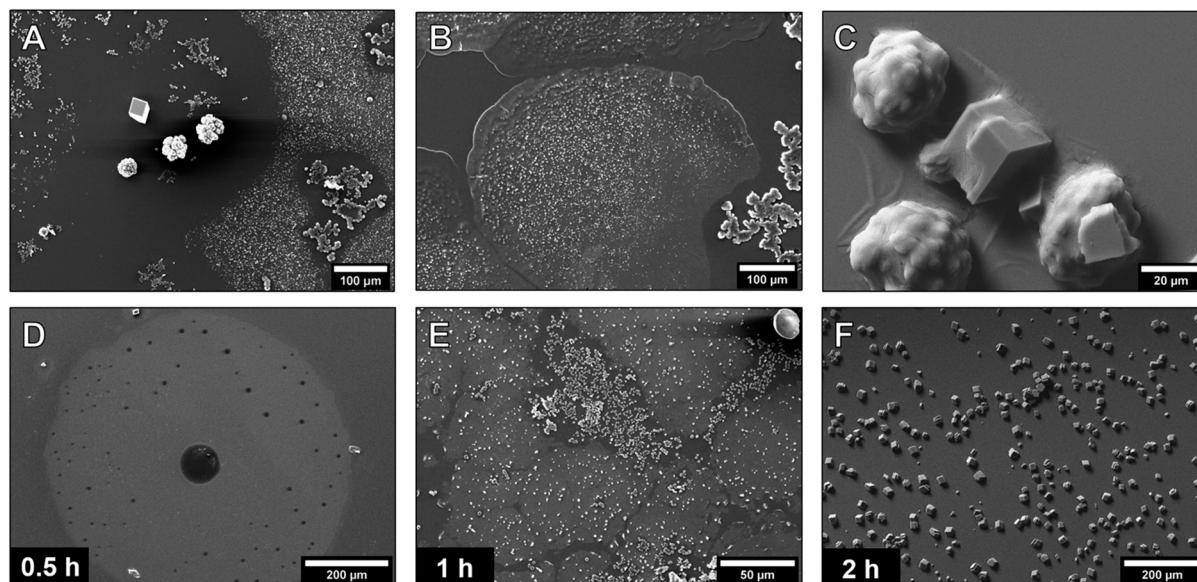
Fig. 3 SEM images for 1 h additive-free gas diffusion experiments using A) 10 mM, B) 20 mM and C) 40 mM CaCl₂. A) Different structures are visible on the wafer. No films or smaller particles are visible around larger amorphous or crystalline structures, therefore, likely a dissolution–reprecipitation mechanism occurs. B) In many areas of the wafer, large films with smooth edges were detected. Closer to the center of the spherical structures, smaller particles are visible. C) Calcite and vaterite particles are covered by the film. D)–F) Time-dependent development of the precursor films in the additive-free experiments using 10 mM CaCl₂.

150 nm-sized particles. The amorphous particles then dissolved and reprecipitated to form larger amorphous structures with a size of 10 to 50 μm (Fig. S8†). The film breaking apart to particles is a rather compelling proof for the liquid nature of the precursor structures based on thermodynamics of phase transformations.[9] It would be thermodynamically impossible for a macroscopic, solid ACC film of 100 nm thickness to transform into smaller ACC nanoparticles, as this would

correspond to anti-Ostwald ripening. It is possible for liquids, however, as liquids can change their composition drastically and macroscopic dense liquid films are metastable with respect to ACC nanoparticles.

When the experimental conditions were changed, *e.g.*, droplets with a larger volume were used, no large films were visible to the naked eye in additive-stabilized systems. This indicates that droplet surface area, surface tension, diffusion barriers and used concentrations determine whether large precursor films are detectable or not, which might be the reason why this effect was not reported in the literature before. Even if no large films are detected, LLPS is still expected to take place in gas diffusion experiments, although the liquid species could occur in different forms, such as dispersed liquid (nano-)droplets (Fig. 4).[43,44]

Conclusions

Our results confirm and visualize the dense liquid calcium carbonate precursor phase in the absence (and presence) of additives. This is possible due to the precursors exhibiting sufficient kinetic stability in gas-diffusion-based syntheses to be detected. Thus, it is important to consider liquid precursor species for the discussion of diffusion-based experiments, even if no stabilizing additives are present. Liquid species and their interactions with additives open a new perspective on crystallization processes of minerals and beyond. Exploiting the liquid properties of mineral precursors can be used to synthesize new materials. In addition, we present an advancement of the ammonia diffusion method that can be employed to address various
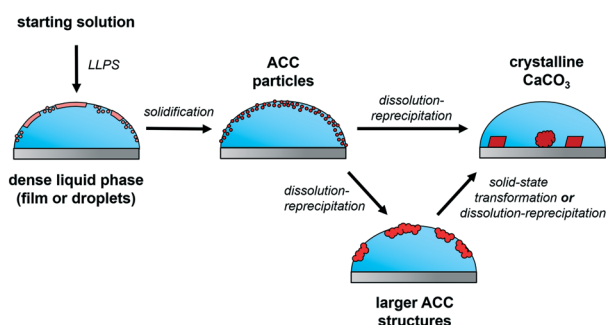
Fig. 4 The proposed mechanism of CaCO₃ crystallization in diffusion-based experiments. The first phase separation in the system is LLPS forming a dense liquid mineral phase. This phase can appear as a film or droplets, depending on the experimental conditions. The liquid precursor phase then solidifies to ACC particles, which in turn dissolve to form larger amorphous structures or directly the crystalline polymorphs. In parallel with the processes shown, ACC particles could form in the solution or crystalline calcium carbonates on the surface of the wafer can occur (not shown in the scheme). Solid-state transformations were also observed for the dried ACC precipitates (Fig. S12†).

questions in carbonate material syntheses. Besides detection and isolation of transient phases, this method can help to optimize synthesis conditions in the ADM by allowing efficient screening of large arrays of experimental parameters and allows the economical use of additives due to the low volumes of the experiments.

Experimental section

Gas diffusion mineralization experiments

The experiments were carried out using 24 cell culture microwell plates. Each chamber was covered with a lid with a hole of 0.5 mm in diameter. Inside each chamber, a 5×5 mm Si-wafer (TED PELLA, Inc.) was placed, on which 20 µL of calcium chloride solution (prepared by dilution of 1 M stock solution, VWR AVS Titrinorm) was pipetted. Depending on the type of experiment, droplets with different $CaCl_2$ concentrations (10 mM to 40 mM) and PAA concentrations (0 g L^{-1} to 1 g L^{-1}, Sigma-Aldrich, poly(acrylic acid) DDMAT terminated, M_n = 7800 g mol^{-1}) were used. For experiments longer than 2 h, a 5×5 mm glass wafer (cut from VWR microscope slides) was used as a substrate. Then, 0.5 g of freshly ground ammonium carbonate (Sigma-Aldrich, ≥30% NH_3-basis) was placed inside a petri dish with a cap containing three holes (1 mm diameter) inside a desiccator (2.4 dm^3 internal volume). The well-plate with the $CaCl_2$ solutions was placed on top of the porcelain plate in the desiccator and the desiccator was closed. Experiments ran from 30 min up to 24 h, as stated. Once the experiments were finished, the well plate was removed from the desiccator and the solution was immediately removed using filter paper. Removal of the solvent usually took no longer than 5 min. The wafers were dried in air overnight and characterized. Each experiment was performed at least twice to confirm reproducibility. All aqueous solutions were prepared using Milli-Q water that was degassed by bubbling nitrogen through the solution overnight.

Characterization

Scanning electron microscopy (SEM) images of the dried wafers were recorded using a JEOL JSM-6610 SEM. The wafers were coated with gold (5–10 nm thick layer) prior to analysis. Attenuated-total-reflection Fourier-transform infrared (ATR-FTIR) spectra were measured using a BRUKER Tensor 27 FTIR spectrometer. The wafers with the calcium carbonate precipitates were directly put on the ATR unit of the spectrometer. The respective wafer (Si or glass) was used as a background reference. Light microscopy was performed on a Keyence VHX-600 Digital Microscope equipped with a VHZ100UR Zoom Lens.

Conflicts of interest

There are no conflicts to declare.

Acknowledgements

References

1 F. C. Meldrum and H. Cölfen, *Chem. Rev.*, 2008, **108**, 4332–4432.

2 L. Addadi, J. Moradian, E. Shay, N. Maroudas and S. Weiner, *Proc. Natl. Acad. Sci. U. S. A.*, 1987, **84**, 2732–2736.

3 J. Ihli, P. Bots, A. Kulak, L. G. Benning and F. C. Meldrum, *Adv. Funct. Mater.*, 2013, **23**, 1965–1973.

4 P. J. Smeets, K. R. Cho, R. G. Kempen, N. A. Sommerdijk and J. J. De Yoreo, *Nat. Mater.*, 2015, **14**, 394–399.

5 P. J. Smeets, K. R. Cho, N. A. Sommerdijk and J. J. De Yoreo, *Adv. Funct. Mater.*, 2017, **27**, 1701658.

6 Y. Y. Kim, C. L. Freeman, X. Gong, M. A. Levenstein, Y. Wang, A. Kulak, C. Anduix-Canto, P. A. Lee, S. Li, L. Chen, H. K. Christenson and F. C. Meldrum, *Angew. Chem., Int. Ed.*, 2017, **56**, 11885–11890.

7 Y. Y. Kim, L. A. Fielding, A. N. Kulak, O. Nahi, W. Mercer, E. R. Jones, S. P. Armes and F. C. Meldrum, *Chem. Mater.*, 2018, **30**, 7091–7099.

8 J. Ihli, J. N. Clark, N. Kanwal, Y. Y. Kim, M. A. Holden, R. J. Harder, C. C. Tang, S. E. Ashbrook, I. K. Robinson and F. C. Meldrum, *Chem. Sci.*, 2019, **10**, 1176–1185.

9 C. Ruiz-Agudo, J. Lutz, P. Keckeis, M. King, A. Marx and D. Gebauer, *J. Am. Chem. Soc.*, 2019, **141**, 12240–12245.

10 J. Ihli, M. A. Levenstein, Y. Y. Kim, K. Wakonig, Y. Ning, A. Tatani, A. N. Kulak, D. C. Green, M. Holler, S. P. Armes and F. C. Meldrum, *Chem. Sci.*, 2020, **11**, 355–363.

11 Y. Ning, F. C. Meldrum and S. P. Armes, *Chem. Sci.*, 2019, **10**, 8964–8972.

12 M. Douverne, Y. Ning, A. Tatani, F. C. Meldrum and S. P. Armes, *Angew. Chem., Int. Ed.*, 2019, **58**, 8692–8697.

13 Y. Ning, L. Han, M. J. Derry, F. C. Meldrum and S. P. Armes, *J. Am. Chem. Soc.*, 2019, **141**, 2557–2567.

14 Y. Ning, L. Han, M. Douverne, N. J. Penfold, M. J. Derry, F. C. Meldrum and S. P. Armes, *J. Am. Chem. Soc.*, 2019, **141**, 2481–2489.

15 Y. Y. Kim, R. Darkins, A. Broad, A. N. Kulak, M. A. Holden, O. Nahi, S. P. Armes, C. C. Tang, R. F. Thompson, F. Marin, D. M. Duffy and F. C. Meldrum, *Nat. Commun.*, 2019, **10**, 5682.

16 J. Ihli, D. C. Green, C. Lynch, M. A. Holden, P. A. Lee, S. Zhang, I. K. Robinson, S. E. D. Webb and F. C. Meldrum, *Angew. Chem., Int. Ed.*, 2019, **58**, 17328–17334.

17 Y. Y. Kim, J. D. Carloni, B. Demarchi, D. Sparks, D. G. Reid, M. E. Kunitake, C. C. Tang, M. J. Duer, C. L. Freeman, B. Pokroy, K. Penkman, J. H. Harding, L. A. Estroff, S. P. Baker and F. C. Meldrum, *Nat. Mater.*, 2016, **15**, 903–910.

18 Z. Dong, L. Feng, Y. Hao, M. Chen, M. Gao, Y. Chao, H. Zhao, W. Zhu, J. Liu and C. Liang, *J. Am. Chem. Soc.*, 2018, **140**, 2165–2178.

19 L. B. Gower and D. J. Odom, *J. Cryst. Growth*, 2000, **210**, 719–734.

20 Y. Xu, K. C. H. Tijssen, P. H. H. Bomans, A. Akiva, H. Friedrich, A. P. M. Kentgens and N. Sommerdijk, *Nat. Commun.*, 2018, **9**, 2582.

21 S. Yao, X. Lin, Y. Xu, Y. Chen, P. Qiu, C. Shao, B. Jin, Z. Mu, N. A. Sommerdijk and R. Tang, *Adv. Sci.*, 2019, **6**, 1900683.

22 M. Bacino, V. Girn, H. Nurrohman, K. Saeki, S. J. Marshall, L. Gower, E. Saeed, R. Stewart, T. Le and G. W. Marshall, *Dent. Mater.*, 2019, **35**, 53–63.

23 C. Jenewein, C. Ruiz-Agudo, S. Wasman, L. Gower and H. Cölfen, *CrystEngComm*, 2019, **21**, 2273–2280.

24 F. Sebastiani, S. L. Wolf, B. Born, T. Q. Luong, H. Cölfen, D. Gebauer and M. Havenith, *Angew. Chem., Int. Ed.*, 2017, **56**, 490–495.

25 J. T. Avaro, S. L. P. Wolf, K. Hauser and D. Gebauer, *Angew. Chem., Int. Ed.*, 2020, **59**, 6155–6159.

26 D. Gebauer, A. Völkel and H. Cölfen, *Science*, 2008, **322**, 1819–1822.

27 H. Du, C. Courregelongue, J. Xto, A. Bohlen, M. Steinacher, C. N. Borca, T. Huthwelker and E. Amstad, *Chem. Mater.*, 2020, **32**, 4282–4291.

28 A. R. Finney, R. Innocenti Malini, C. L. Freeman and J. H. Harding, *Cryst. Growth Des.*, 2020, **20**, 3077–3092.

29 M. A. Bewernitz, D. Gebauer, J. Long, H. Cölfen and L. B. Gower, *Faraday Discuss.*, 2012, **159**, 291–312.

30 S. E. Wolf, L. Müller, R. Barrea, C. J. Kampf, J. Leiterer, U. Panne, T. Hoffmann, F. Emmerling and W. Tremel, *Nanoscale*, 2011, **3**, 1158–1165.

31 A. F. Wallace, L. O. Hedges, A. Fernandez-Martinez, P. Raiteri, J. D. Gale, G. A. Waychunas, S. Whitelam, J. F. Banfield and J. J. De Yoreo, *Science*, 2013, **341**, 885–889.

32 L. B. Gower, *Chem. Rev.*, 2008, **108**, 4551–4627.

33 S. E. Wolf, J. Leiterer, M. Kappl, F. Emmerling and W. Tremel, *J. Am. Chem. Soc.*, 2008, **130**, 12342–12347.

34 M. H. Nielsen, S. Aloni and J. J. De Yoreo, *Science*, 2014, **345**, 1158–1162.

35 Z. Zou, W. J. Habraken, L. Bertinetti, Y. Politi, A. Gal, S. Weiner, L. Addadi and P. Fratzl, *Adv. Mater. Interfaces*, 2017, **4**, 1600076.

36 J. Aizenberg, S. Albeck, S. Weiner and L. Addadi, *J. Cryst. Growth*, 1994, **142**, 156–164.

37 S. J. Homeijer, M. J. Olszta, R. A. Barrett and L. B. Gower, *J. Cryst. Growth*, 2008, **310**, 2938–2945.

38 Y. Han, T. Nishimura and T. Kato, *Polym. J.*, 2014, **46**, 499–504.

39 Y.-Y. Kim, E. P. Douglas and L. B. Gower, *Langmuir*, 2007, **23**, 4862–4870.

40 H. Du, C. Courrégelongue, J. Xto, A. Böhlen, M. Steinacher, C. N. Borca, T. Huthwelker and E. Amstad, *Chem. Mater.*, 2020, **32**, 4282–4291.

41 H. Du, M. Steinacher, C. Borca, T. Huthwelker, A. Murello, F. Stellacci and E. Amstad, *J. Am. Chem. Soc.*, 2018, **140**, 14289–14299.

42 H. Du and E. Amstad, *Angew. Chem., Int. Ed.*, 2020, **59**, 1798–1816.

43 J. Rieger, T. Frechen, G. Cox, W. Heckmann, C. Schmidt and J. Thieme, *Faraday Discuss.*, 2007, **136**, 265–277.

44 P. J. M. Smeets, A. R. Finney, W. J. E. M. Habraken, F. Nudelman, H. Friedrich, J. Laven, J. J. De Yoreo, P. M. Rodger and N. A. J. M. Sommerdijk, *Proc. Natl. Acad. Sci. U. S. A.*, 2017, **114**, E7882–E7890.